Extreme Electrostatic Phenomena in a Single Sonoluminescing Bubble

Ning Xu,[1] Long Wang,[1] and Xiwei Hu[2]
[1]*Institute of Physics, Chinese Academy of Sciences, Beijing 100080, People's Republic of China*
[2]*University of Science and Technology of China, Hefei 230026, People's Republic of China*
(Received 8 September 1998)

A multihydrodynamic model is established to simulate a sonoluminescing argon bubble. The results show that a partially ionized plasma layer is generated and contributes to the flash by assumed thermal bremsstrahlung. A strong electric field of up to 2×10^{10} V/m, caused by the plasma dipole diffusion, emerges along the shock front. The spike of the electric field helps prevent the occurrence of Rayleigh-Taylor instability and thus maintains perfect spherical symmetry of the shocks. This may be a key reason for the over 12 orders of magnitude sound-energy concentration.

PACS numbers: 78.60.Mq, 47.40.–x, 34.80.Dp

A gas bubble levitating in a liquid trapped and driven by a periodic acoustic field may generate a flash with a measured pulse width from under 40 to over 350 ps [1], which is the well known but still mysterious sonoluminescence (SL) [2]. This peculiar phenomenon has been measured frequently [1,3–9] since the first procurement of a single sonoluminescing bubble by Gaitan *et al.* [10]. Theoretical studies using hydrodynamic models [11,12] have suggested that shock waves generate and propagate in the bubble during the final collapse of the bubble wall, which compress and heat the gases to a kind of waterlike or solidlike and partially ionized high temperature plasma, and light is emitted due to the existence of this plasma. Recent numerical studies of the pulse width and spectra of single bubble sonoluminescence (SBSL) [13] and experiment [1] strongly support the plasma explanation of SL.

Shock induced charge separation and the high intensity electric field have been studied theoretically [14]. While a partially ionized multicomponent plasma exists in the shock front of a sonoluminescing bubble, electrons, various ions, and atoms will exhibit different hydrodynamic and transport behavior. Electrons will move from the plasma center to the edge much faster than ions and atoms. This will lead to charge separation and establish a pair of local electric currents, hence a double layer of charge and an electric field. Because of the extremely high density of the charged particles [15] and the very thin shock front during the final violent collapse of the bubble gases, even feeble charge separation could engender considerable electric field and intense local electric current. Our calculations affirm this surmise, from which we find that (i) an inhomogeneous plasma layer with high density is generated, which results in charge separation on account of the dipole diffusion; (ii) a strong electric field spike with short time duration and narrow spatial resolution emerges during the final collapse of the bubble; (iii) this electric field spike may stabilize the Rayleigh-Taylor instability along the shock front and maintain the shock waves in a perfect spherical symmetry, which might be a key reason for the high energy concentration.

We take a pure argon bubble levitating in water as our study object, and assume spherical symmetry of the bubble with ambient radius R_0. The acoustic pressure $P_a(t) = -P_a \sin\omega_a t$ and the ambient pressure $P_0 = 1$ atm form the driving pressure applied to the bubble wall, where P_a and ω_a are the amplitude and frequency of the acoustic pressure. The typical parameters adopted in our computations are $R_0 = 4.5$ μm, $P_a = 1.425$ atm, and $\omega_a = 2\pi \times 26.5$ kHz. Since the ion-electron collision time is very short compared with the SL duration [13], different kinds of particles will soon reach the same temperature locally. All the particles in each fluid element thus have the same temperature.

We consider only one cycle of the repetitive oscillations. Driven by the oscillatory pressure, the bubble wall moves according to the Rayleigh-Plesset equation [11]

$$R\ddot{R} + \frac{3}{2}\dot{R}^2 = \frac{1}{\rho_l}[P(R,t) - P_a(t) - P_0] + \frac{R}{\rho_l c_l}\frac{d}{dt} \times [P(R,t) - P_a(t)] - 4\nu\frac{\dot{R}}{R}, \quad (1)$$

where R is the bubble radius, overdots denote differentiation with respect to time, $P(R,t)$ is the gas pressure next to the bubble wall, ρ_l is the density of the water, c_l is the speed of sound in water, and ν is the kinematic viscosity of the water. The bubble is treated as an airtight system comprising different kinds of particles such as atoms, ions, and electrons, while the surface tension, thermal conductivity, and viscosity are all neglected. For this multifluid system, we employ the following equations of continuity and motion, and the Poisson equation:

$$\frac{\partial\rho_i}{\partial t} + \nabla\cdot(\rho_i\mathbf{v}_i) = \frac{\delta\rho_i}{\delta t}, \quad (2)$$

$$\frac{\partial(\rho_i\mathbf{v}_i)}{\partial t} + \nabla\cdot(\rho_i\mathbf{v}_i\mathbf{v}_i) = -\nabla(P_i + Q_i) + Z_i e n_i\mathbf{E} + \mathbf{M}_i, \quad (3)$$

$$\nabla\cdot\mathbf{E} = 4\pi\sum_i (Z_i e n_i), \quad (4)$$

where ρ_i, $\mathbf{v}_i$, P_i, Q_i, n_i, $Z_i e$, and $\mathbf{M}_i$ are, respectively, the density, velocity, pressure, artificial viscosity, number density, charge, and friction force of the ith particles (electrons, $i = e$; atoms, $i = 0$; ions, $i = 1, 2, \ldots, 5$); here $\mathbf{E}$ is the electric field caused by charge separation, and $\delta\rho_i/\delta t$ is the rate of change of ρ_i due to inelastic collisions. Here we only consider ions with the highest charge of five, because high levels of ionization are relatively very weak. The inelastic processes considered in this paper are electron collisional ionization, radiative recombination, and three-body recombination, therefore, for atoms and ions, $\delta\rho_i/\delta t$ is commonly expressed as [15]

$$\frac{\delta\rho_i}{\delta t} = m_i[n_{i-1}n_e\alpha^{\text{ion}}_{i-1\to i} - n_i n_e \alpha^{\text{ion}}_{i\to i+1} + n_{i+1}n_e(\alpha^{\text{rrec}}_{i+1\to i} + \alpha^{\text{trec}}_{i+1\to i}) - n_i n_e(\alpha^{\text{rrec}}_{i\to i-1} + \alpha^{\text{trec}}_{i\to i-1})], \qquad (i = 0, 1, \ldots, 5), \tag{5}$$

where m_i is the mass of a particle, and $\alpha^{\text{ion}}_{i\to i+1}$, $\alpha^{\text{rrec}}_{i\to i-1}$, and $\alpha^{\text{trec}}_{i\to i-1}$ represent the rates of ionization, radiative recombination, and three-body recombination of particles with the charge of i, which are given by [16–18]

$$\alpha^{\text{ion}}_{i\to i+1} = 10^{-5}\,\frac{(T/I_i)^{1/2}}{(I_i)^{3/2}(6.0 + T/I_i)}\exp(-I_i/T)\ [\text{cm}^3\,\text{s}^{-1}], \tag{6}$$

$$\alpha^{\text{rrec}}_{i\to i-1} = -1.8645 \times 10^{-12}(i)^4(\mu_i c^2)^{-1/2}(kT)^{-3/2}e^{1/\chi}E_i(-1/\chi)S(\chi)\ [\text{cm}^3\,\text{s}^{-1}], \tag{7}$$

$$\alpha^{\text{trec}}_{i\to i-1} = \frac{5.25 \times 10^{-27}}{(T/1000)^{3/2}}\,n_e\,\frac{g_i}{g_{i-1}}\exp(I_{i-1}/T)\alpha^{\text{ion}}_{i-1\to i}\ [\text{cm}^3\,\text{s}^{-1}], \tag{8}$$

where

$$S(\chi) = \begin{cases} 0.704 - 1.146\log_{10}\chi, & \text{if } \chi \le 10^{-2}, \\ 1.592 - 0.340\log_{10}\chi + 0.113\log^2_{10}\chi & \\ \quad -0.031\log^3_{10}\chi + 0.003\log^4_{10}\chi, & \text{if } 10^{-2} < \chi \le 10^6, \\ 2.302\chi^{-0.107}, & \text{if } \chi > 10^6, \end{cases} \tag{9}$$

$$E_i(-1/\chi) = -\ln\chi + \gamma + \sum_{n=1}^{\infty}\frac{(-1)^n}{nn!\,\chi^n}. \tag{10}$$

I_i is the ionization energy (in eV), $\chi = kT/E_{si}$, $E_{si} = \frac{1}{2}(i/\alpha)^2\mu_i c^2$, μ_i is the reduced mass of an electron and an ion, $\alpha = 1/137.036$ is the fine-structure constant, γ is Euler's constant, and the g's are statistical weights. Temperature T is expressed in eV in Eqs. (6) and (8), while in degrees Kelvin in Eq. (7). The $\delta\rho_e/\delta t$ can be obtained by mass conservation. The energy equation of the system as a whole is

$$\frac{\partial(\rho\epsilon)}{\partial t} + \sum_i[\nabla\cdot(\rho\epsilon_i\mathbf{v}_i)] = \sum_i\left[-(P_i + Q_i)\nabla\cdot\mathbf{v}_i + \frac{1}{2}\,v_i^2\,\frac{\delta\rho_i}{\delta t}\right] + W - U_r, \tag{11}$$

where ϵ_i is the internal energy of particles of species i, $\rho = \sum_i \rho_i$ and $\epsilon = \sum_i \epsilon_i$ are the total density and internal energy, W is the heat generated from the collision among different species of particles [19], and U_r is the energy loss rate due to radiation. Here we assume bremsstrahlung to be the cause of SL, which is also supported by recent experiments [1]. We adopt the equation of state appropriate for dense gases and include ionization in it, assuming the ionization energy originates mainly from electrons [20],

$$P_i = \frac{n_i kT}{1 - b\rho}, \tag{12}$$

$$\epsilon_i = \frac{3}{2}\,\frac{n_i kT}{\rho}, \qquad (i = 0, 1, \ldots, 5), \tag{13}$$

$$P_e = \frac{n_e kT}{1 - b\rho}, \tag{14}$$

$$\epsilon_e = \frac{1}{\rho}\left(\frac{3}{2}\,n_e kT + E_I\right), \tag{15}$$

where k is the Boltzmann constant, T is the temperature, b is the van der Waals excluded volume which avoids the gases being infinitely compressed, and E_I is the ionization energy. All the equations listed above form a complete and self-consistent numerical problem to describe the gas motion in the bubble.

Figure 1 is the time evolution of the shocks and the induced electric field. The six curves delineate the profiles of the quantities at six instants during the final collapse of the bubble. Figure 1(A) shows the shock propagation, which is qualitatively the same as what has been discussed elsewhere, where $v = |\mathbf{v}|$ is the mean velocity of a fluid element, satisfying the relation: $\rho\mathbf{v} = \sum_i \rho_i\mathbf{v}_i$. As the bubble wall collapses and reaches the velocity above 1 M, shock waves emerge and violently rush to the center of the bubble. Shocks are strengthened during propagation, compressing the gases to high enough temperatures to ionize. Driven by the gradients of temperature, pressure and density, particles will diffuse, leading to the rearrangement of the distribution of the plasma in space. The plasma region is thus obviously broadened. The diffusion is one reason for the energy loss, which makes the temperature drop, and thus ions with high charge numbers are no longer the main ingredients of the plasma. The highest temperature that we get is about 20 eV, which is close to the estimates by experiments. Because

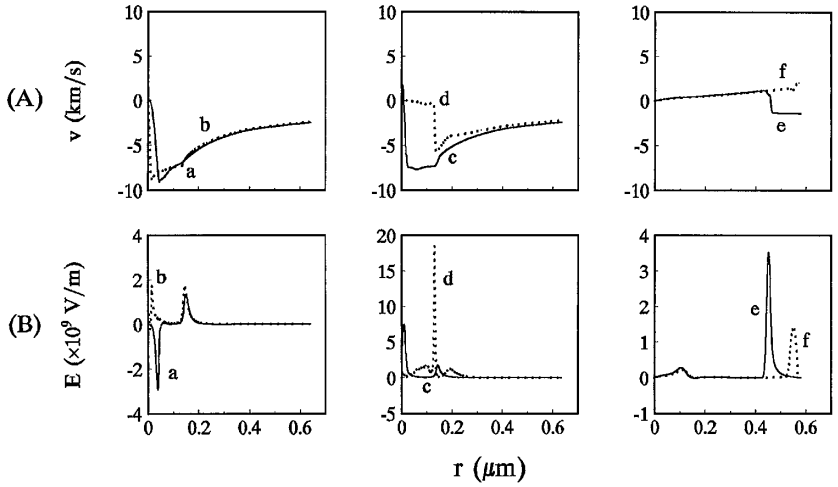

FIG. 1. Simulated temporal evolution of the velocity (v) and the electric field (E) over a time duration of 44.3 ps. The six curves marked as "a"–"f" represent spatial profiles of the quantities at six instants: (a) $t_a = 22.428\,993\,2$ μs; (b) $t_b = t_a + 2.6$ ps; (c) $t_c = t_a + 3.0$ ps; (d) $t_d = t_a + 9.5$ ps; (e) $t_e = t_a + 31.2$ ps; (f) $t_f = t_a + 44.3$ ps.

of their tiny masses, electrons diffuse to the edges of the plasma area much faster than the ions and atoms, and the separation of charged particles leads to the local accumulation of charges. The electric field is thus generated, decelerating the motion of electrons and accelerating that of ions, which is called dipole electric field in the plasma. Figure 1(B) shows the time evolution of the electric field. A sharp spike higher than 1×10^9 V/m emerges and moves with the shock front during the final collapse of the bubble wall. As the second shock rebounds from the center of the bubble, the highest electric field reaches about 2×10^{10} V/m. Compared with the electric field at the Bohr radius of a hydrogen nucleus ($E_B \approx 5 \times 10^{11}$ V/m), such an electric field has approximately reached the lower threshold of the so-called strong laser electric field (the corresponding intensities are $I \approx 10^{14}$ W/cm^2 and $I_B \approx 3 \times 10^{16}$ W/cm^2, respectively).

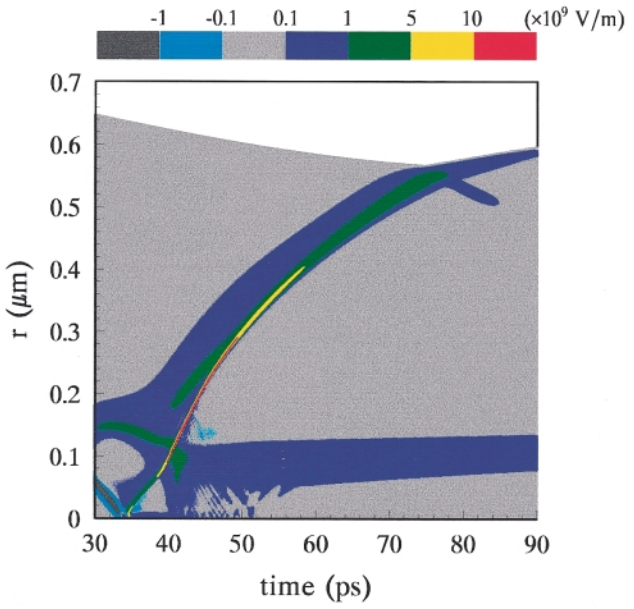

FIG. 2 (color). The time-space evolution of the electric field in the final 60 ps. Different colors represent different ranges of electric field intensity. The instant time = 0 here represents $t = 22.4289$ μs.

Figure 2 shows the time-space evolution of the electric field. The time dependence of the bubble radius can be seen from the upper boundary of the colored area. The red line shaped area describes the electric field above 1×10^{10} V/m. It goes through about 20 ps and is about tens of nanometers wide. An electric field above 1×10^9 V/m accompanies the main process of SL. Can a sonoluminescing bubble be another source of the strong field besides an ultrashort pulsed laser? If this hypothesis is feasible, a completely new and interesting field may evolve for the applications of SL.

Figure 3 shows the light power, with a wavelength from 180 to 750 nm, calculated by assuming bremsstrahlung as the mechanism of the radiation. The maximum power in our case is about 19 mW, and the full width at half maximum (FWHM) of the pulse is about 33 ps. The diffusion of plasma components also broadens the region contributing to SL, compared with what was obtained by treating all the plasma components as a unity [15]. Although the temperatures are much lower than those given in previous studies, the light intensity is not markedly influenced because of this extension, and the plasma is shown to

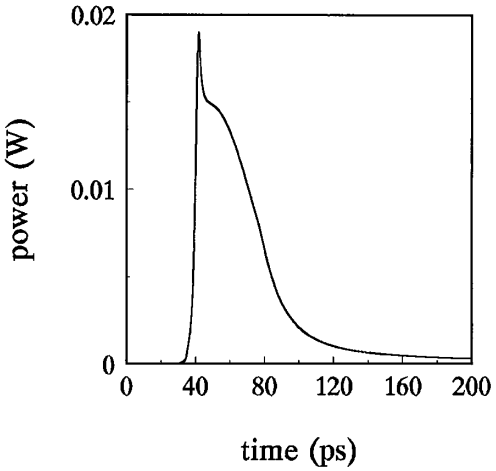

FIG. 3. The emission power of the sonoluminescing bubble in the final 200 ps starting from $t = 22.4289$ μs. The wavelength range of the light calculated here is from 180 to 750 nm.

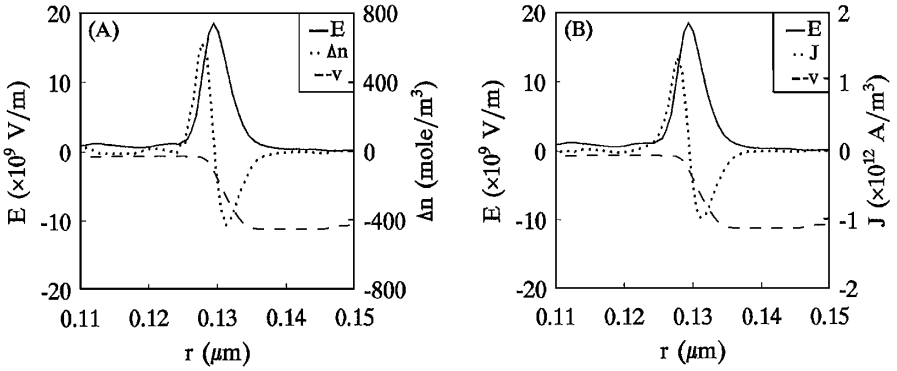

FIG. 4. Profiles of the charge number density (Δn), electric field (E), and electric current density (J) striding on the shock front at the moment (same as t_d in Fig. 1) near the emergence of the maximum electric field.

be completely optical thin for bremsstrahlung. Thermal plasma conduction is considered to be an important mechanism of the picosecond pulse width and the absence of the "afterglow" [13]. The "tail" of the calculated output may be eliminated if the thermal conduction is involved.

In the extreme environment of SL, can the shock waves be stable? If there are some disturbances, the sharp gradients of the thermodynamic quantities along the shock front may cause Rayleigh-Taylor instability and destroy the spherical symmetry of an imploding shock. Some corresponding effects, e.g., filamentary electron jets, will thus be generated. However, a strong electric field can prohibit the Rayleigh-Taylor instability caused by electron disturbances. Figure 4 shows the phases of the concerned quantities at the moment near the emergence of the maximum electric field. Propelled by the shocks, electrons move much faster than ions; therefore, electrons will amass in front of the shock front and leave ions behind. This accumulation leads to the "double-layer" charge distribution [Fig. 4(A)]. The electric field spike thus emerges, striding on the shock front. A similar profile for the electric current density is presented in Fig. 4(B). The acceleration of electrons caused by the electric field is $\mathbf{a}_E = -e\mathbf{E}/m_e$, where m_e is the mass of an electron. It is obvious that $\mathbf{a}_E$ is opposite to $\mathbf{E}$ in direction, which determines that the electric field spike will hinder the motion of the electrons before the shock front. When the nonspherical disturbances of electron flux occur at the shock front, the strong electric field will automatically drag the electron flux back, and thus retain the perfect spherical symmetry of the shock waves. This may be one of the key factors for efficient shock implosion and the over 12 orders of magnitude sound-energy concentration. A detailed study of the instability caused by the electric field gradient will be discussed later.

Because of the tiny size of the bubble and the transient properties of SL, it is difficult to detect what is exactly in the sonoluminescing bubble. Our model includes a more complete description of the processes of implosion and predicts the existence of a strong electric field. We also indicate the effects of this strong electric field on the Rayleigh-Taylor instability. This kind of strong electric field may have other effects, e.g., the polarization and field ionization of molecules and atoms, and the potentially new kinds of radiation. All these may help further our understanding of this fascinating bubble.

This research is supported partly by the National High-Tech ICF committee in China and by NSFC No. 19875052.

[1] R. A. Hiller, S. J. Putterman, and K. R. Weninger, Phys. Rev. Lett. **80**, 1090 (1998).
[2] B. P. Barber *et al.*, Phys. Rep. **281**, 65 (1997).
[3] B. P. Barber and S. J. Putterman, Nature (London) **352**, 318 (1991).
[4] R. Hiller, S. J. Putterman, and B. P. Barber, Phys. Rev. Lett. **69**, 1182 (1992).
[5] B. P. Barber and S. J. Putterman, Phys. Rev. Lett. **69**, 3839 (1992).
[6] B. P. Barber, C. C. Wu, R. Löfstedt, P. H. Roberts, and S. J. Putterman, Phys. Rev. Lett. **72**, 1380 (1994).
[7] R. Hiller, K. Weninger, S. J. Putterman, and B. P. Barber, Science **266**, 248 (1994).
[8] K. R. Weninger, B. P. Barber, and S. J. Putterman, Phys. Rev. Lett. **78**, 1799 (1997).
[9] B. Gompf *et al.*, Phys. Rev. Lett. **79**, 1405 (1997).
[10] D. F. Gaitan and L. A. Crum, J. Acoust. Soc. Am. Suppl. **87**, S141 (1990).
[11] C. C. Wu and P. H. Roberts, Phys. Rev. Lett. **70**, 3424 (1993).
[12] W. C. Moss, D. B. Clarke, J. W. White, and D. A. Young, Phys. Fluids **6**, 2979 (1994).
[13] W. C. Moss, D. B. Clarke, and D. A. Young, Science **276**, 1398 (1997).
[14] O. W. Greenberg, H. K. Sen, and Y. M. Treve, in *Proceedings of the Fourth International Conference on Ionization Phenomena in Gases, 1959* (North-Holland, Amsterdam, 1960), Vol. II, p. 1098.
[15] Ning Xu, Long Wang, and Xiwei Hu, Phys. Rev. E **57**, 1615 (1998).
[16] D. L. Book, *NRL Plasma Formulary* (Naval Research Laboratory, Washington, DC, 1987), p. 54.
[17] A. Erdas and P. Quarati, Z. Phys. D **28**, 185 (1993).
[18] D. E. Post *et al.*, At. Data Nucl. Data Tables **20**, 398 (1977).
[19] S. I. Braginskii, *Transport Processes in A Plasma*, Reviews of Plasma Physics Vol. 1 (Consultants Bureau, New York, 1965).
[20] R. M. More, *Physics of Laser Plasma*, Handbook of Plasma Physics Vol. 3 (North-Holland, Amsterdam, 1991), Chap. 2.